Letters

Integrated Common-Mode Filter for GaN Power Module With Improved High-Frequency EMI Performance

Niu Jia, *Graduate Student Member, IEEE*, Xingyue Tian, *Graduate Student Member, IEEE*, Lingxiao Xue, *Senior Member, IEEE*, Hua Bai, *Senior Member, IEEE*, Leon M. Tolbert, *Fellow, IEEE*, and Han Cui, *Senior Member, IEEE*

***Abstract*—While the employment of wide bandgap (WBG) devices in high-frequency and high-voltage applications brings benefits such as reduced system size and improved efficiency, it aggravates the electromagnetic interference (EMI) issue due to fast switching. High-frequency EMI noise suppression relies mainly on the filter design, where the filter's performance is strongly affected by parasitics. Through analyzing the common-mode (CM) equivalent circuit of a half-bridge power module, this letter identifies the key parasitics that dominate the performance of a common-mode filter (CMF) at high frequencies. To minimize the parasitics, the concept of integrating the CMF inside the WBG power module package is developed to improve the noise attenuation. A π-type CMF is integrated with a half-bridge GaN-based power module as a prototype to validate the concept. Experiments are conducted by measuring the CM noise spectrum received by the line impedance stabilization networks (LISNs) from the hard switching of the designed power module under 70 V and 80 kHz. Comparing the measured results of the integrated CMF to the externally added CMF, up to 50 dBμV more attenuation is achieved by the integrated CMF in the frequency range of 10 to 100 MHz, verifying the theoretical analysis and the established CM equivalent circuit.**

***Index Terms*—Common mode (CM) noise, electromagnetic interference (EMI), GaN power module package, high frequency, integrated common-mode filter.**

I. Introduction

As wide bandgap (WBG) devices are broadly used in power electronics applications, the system can switch at a higher switching frequency and speed, which yields benefits such as reduced system size and power loss [1], [2]. However, the higher *dv/dt* during switching commutations introduces higher common mode (CM) noise, generating electromagnetic interference (EMI) issues [3]. While the low-frequency EMI noise can be mitigated by methods like active gate drivers and optimized PWM strategies [4], the high-frequency noise such as radiated EMI is strongly affected by parasitics and coupling effects, which create unwanted EMI propagation paths and degrade the EMI performance of the system with established EMI mitigation methods. Therefore, it is crucial to examine the parasitic inductances and capacitances involved in the EMI noise propagation paths in order to optimize the EMI filter's performance in the high-frequency range. For example, the self- and mutual-parasitics effects that lessen the effectiveness of the EMI filter are analyzed in [5], and the corresponding cancellation techniques are discussed to reduce the parasitic impacts and improve the EMI filter's attenuation.

The coupling effects in an active clamp flyback converter are studied from the system level in [3], where the capacitive couplings among different voltage nodes are analyzed such that advantageous couplings for EMI noise attenuation are strengthened while the undesirable couplings are minimized. Improving the noise propagation paths by reducing the parasitics or adding extra filters at the package level has been explored in [6], [7]. Reducing the area of the bottom side of direct bond copper (DBC) and only keeping the effective area needed for the thermal performance effectively reduces the DBC-caused parasitic capacitance, which yields smaller CM noise [6]. Similarly, integrating CM capacitors into a silicon carbide power module reduces conducted EMI by adding low-impedance CM current return paths [7].

The main contribution of this letter is that the concept of integrating common-mode filters (CMF) inside the WBG power module package to improve CM noise reduction is analyzed, demonstrated, and verified through theoretical and experimental results. A theoretical analysis is conducted to explain the rationale of the advantage brought by integration. Section II gives the parasitic analysis of the CM equivalent circuit comparing the power module with a conventional externally added CMF and an integrated CMF. The design and fabrication of the prototype of a GaN power module with an integrated π-type CMF are described in Section III, which is then validated by CM noise measurement under 70-V and 80-kHz continuous hard-switching operations,

Manuscript received 20 December 2022; revised 25 January 2023; accepted 19 February 2023. Date of publication 23 February 2023; date of current version 20 April 2023. This work was supported by the PowerAmerica Member Initiated Projects (MIP3 Subaward No. 2014-0654-85). *(Corresponding author: Han Cui.)*

Niu Jia, Xingyue Tian, Hua Bai, Leon M. Tolbert, and Han Cui are with the Min H. Kao Department of Electrical Engineering and Computer Science, University of Tennessee, Knoxville, TN 37996 USA (e-mail: njia@vols.utk.edu; xtian7@vols.utk.edu; kevinbai@icloud.com; tolbert@utk.edu; helencui@utk.edu).

Lingxiao Xue is with the Oak Ridge National Laboratory, Oak Ridge, TN 37830 USA (e-mail: xuel@ornl.gov).

Color versions of one or more figures in this article are available at https://doi.org/10.1109/TPEL.2023.3248092.

Digital Object Identifier 10.1109/TPEL.2023.3248092

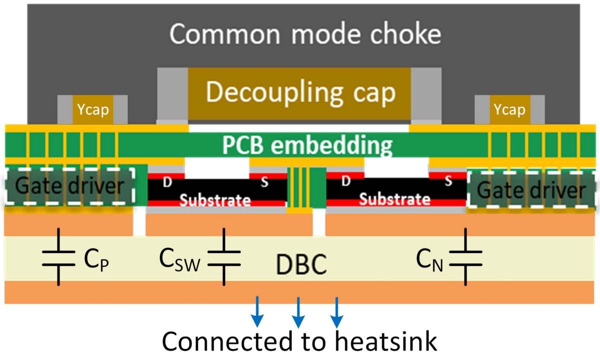

Fig. 1. Designed GaN half-bridge power module package with the integrated CMF.

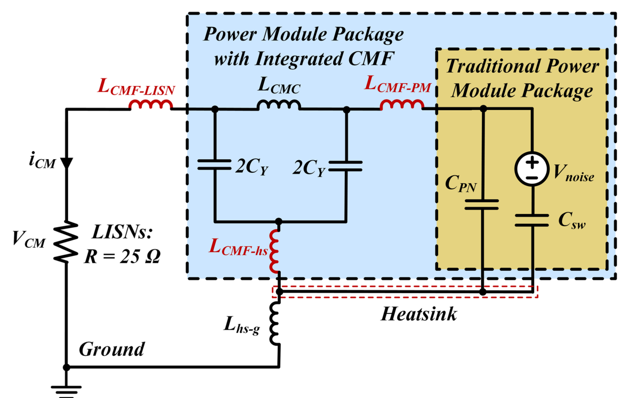

Fig. 2. CM equivalent circuit of the power module with the traditional package and with the CMF-integrated package.

presenting greatly improved high-frequency EMI noise suppression of the integrated filter compared to the external filter. Finally, conclusions are given in Section IV.

II. CM Equivalent Circuit Analysis

This letter uses an equivalent circuit to analyze EMI noises that span the range of both high-frequency conducted EMI (e.g., >10 MHz) and radiated EMI (30–100 MHz). Although the actual radiated EMI noise is measured through receiving antennas, the conducted EMI current in the equivalent circuit as the radiation source is an indicator of the radiated EMI noise level. Therefore, establishing the CM equivalent circuit is useful not only for conducted EMI but also for radiated EMI noise assessment [3], [8]. In the equivalent circuit, the switching devices are represented by equivalent CM voltage noise sources and the EMI propagation paths from the source to the noise receiver (i.e., LISNs) comprising multiple parasitic capacitances and inductances (see Fig. 2) strongly affect the noise reduction results. In a half-bridge power module package as shown in Fig. 1, the CM noise propagates through three main parasitic capacitances: C_P, C_N, and C_{sw}, which are caused by the metal-ceramic-metal sandwich structure of the DBC between the heatsink and *dc*+, *dc*-, and the switching node of the power module, respectively. The inclusion of a CMF in the power conversion system also introduces several main parasitic inductances due to the connections: the parasitic inductance between the line impedance stabilization networks (LISNs) and the CMF $L_{CMF\text{-}LISN}$, the parasitic inductance between the CMF and the power module $L_{CMF\text{-}PM}$, the CMF-to-heatsink parasitic inductance $L_{CMF\text{-}hs}$, and the heatsink-to-ground parasitic inductance $L_{hs\text{-}g}$, assuming that the CMF is grounded through the heatsink of the power module. In this case, the CM equivalent circuit is built as Fig. 2 shows, where C_{PN} is the sum of the paralleled C_P and C_N; L_{CMC} and the two C_Y branches are the CM equivalent model of the π-type CMF, and 25 Ω is the equivalent impedance of the LISNs.

Under high frequency, the impedance of CM choke Z_{CMC} (usually at μH level) is much larger than the impedance of Y-capacitor Z_{CY} (around several nF). Under the assumption of $Z_{CY} \approx 0$, the LISNs' voltage insertion gain (i.e., the noise voltage received by the LISNs' equivalent impedance Z_R over the noise source V_{noise}) can be derived as (1) shown at the bottom of this page, where all the impedances are the corresponding impedances of the parasitics shown in Fig. 2, $Z_{SUM} = Z_R + Z_{hs\text{-}g} + Z_{CMF\text{-}PM} + Z_{CMF\text{-}LISN}$, $\alpha = Z_{CSW}/Z_{CPN}$, and $\eta = Z_{CMF\text{-}PM}/Z_{CMF\text{-}hs}$.

The location of the CMF determines the values of these parasitics. For example, when the CMF is added externally to the power module, the CMF is closer to the LISNs rather than the power module, which equivalently yields smaller $L_{CMF\text{-}LISN}$ and larger $L_{CMF\text{-}PM}$. The connection between the CMF and the heatsink is also longer for the external CMF with a larger $L_{CMF\text{-}hs}$. To compare the external CMF with the integrated CMF, the sum of $L_{CMF\text{-}LISN}$ and $L_{CMF\text{-}PM}$ is kept as a constant, but the value of $L_{CMF\text{-}PM}$ is varied from 0.1 to 450.1 nH to represent the CMF moves further away from the power module. The parasitic inductance $L_{CMF\text{-}hs}$ is also varied accordingly in terms of η. The parametric study results of $Z_{CMF\text{-}PM}$ and $Z_{CMF\text{-}hs}$ in (1) are shown in Fig. 3. In Fig. 3(a), η is kept at unity as an example, and the LISNs' voltage insertion gain reduces significantly with the decrease of $L_{CMF\text{-}PM}$, suggesting that smaller $L_{CMF\text{-}PM}$ and $L_{CMF\text{-}hs}$ enhance the filter's performance on noise suppression along the propagation path. This conclusion is further supported by the four distinct cases with different parasitics shown in Fig. 3(b). In summary, reducing the distance between the CMF and the power module results in lower parasitic inductances that are beneficial for maximizing the noise attenuation for the same filter design.

The analysis above inspires the concept of integrating the CMF into the power module package to minimize the key parasitic inductances and improve the filter performance. Fig. 2

$$G_{LISN} = \frac{Z_R}{(\alpha+1)\left(Z_{SUM}+\eta\left(Z_{SUM}-Z_{CMF-PM}\right)\right)+\alpha Z_{CPN}\left(1+\frac{Z_{SUM}-Z_{CMF-PM}}{Z_{CMF-hs}}\right)} \quad (1)$$

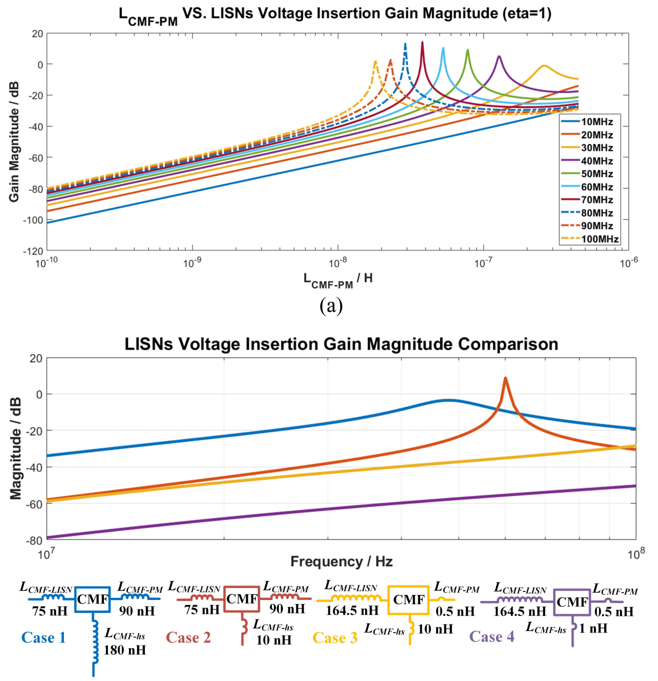

Fig. 3. (a) Impact of $L_{CMF\text{-}PM}$ on the magnitude of LISNs' voltage gain G_{LISN} with $\eta = 1$, (b) Comparison of LISNs' voltage gain with four parasitics conditions from 10 to 100 MHz.

compares the traditional power module package with an externally connected CMF and the power module with an integrated CMF in the package. The traditional power module package only includes the half-bridge switches and the DBC-caused parasitic capacitances, where the CMF placed outside requires long connections to the power module. The proposed power module package with CMF integrated significantly reduces the $L_{CMF\text{-}PM}$ and $L_{CMF\text{-}hs}$ due to shorter connections, which greatly improves the noise reduction at a location adjacent to the noise-generating source. With less noise leaking outside, these "quiet" (e.g., noise free) power modules present great potential in switching at higher frequencies and better noise management capability.

III. Experimental Verification of Integrated Filter

In this section, a prototype is designed for the GaN-based half-bridge power module package with an integrated CMF. A planar CM choke and four capacitors are copackaged with an embedded GaN power module. The module is tested under 70 V and 80 kHz continuous switching, and the measured CM noise spectra from the power module with the integrated filter are compared to those with an external filter and no filter. The experiment result also validates the simulation result of the established CM equivalent circuit discussed in Fig. 2.

A. Design and Fabrication of the GaN Power Module Package With Integrated Filter

Fig. 1 presents the vertical cut view of the designed power module package, adopting low-cost printed circuit board (PCB)

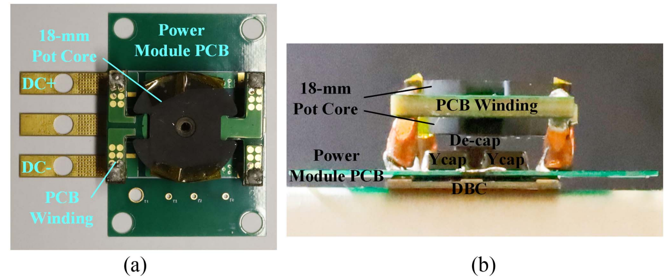

Fig. 4. Prototype for the designed power module package with the integrated CMF. (a) Top view. (b) Side view.

and DBC structure for double-sided cooling, embedding small GaN bare dies for a vertical power loop with high integration of decoupling capacitors, gate drives, and CMF to achieve a high-power density and low-parasitic design [9]. Four Y-capacitors and the decoupling capacitors are soldered on the top side of the PCB, while the GaN dies and integrated gate drives are soldered on the bottom side of the PCB. The CM choke sits on top of the Y-capacitors and the decoupling capacitors.

In [10], a toroidal coupled inductor was used as the CM choke, but it was hard to control the parasitics. To realize better parasitics management, a planar choke with PCB winding is used as the CM choke in this letter. The designed power module with the integrated CMF is shown in Fig. 4. The planar choke consists of a machined 18-mm K1 ferrite pot core and a coupled four-layer PCB winding with two turns per side and one turn per layer. The three-dimensional structures of the windings and cores are simulated in ANSYS HFSS before manufacturing to ensure the impedance is large enough. Both simulation and measurement results show an inductance of 400 nH and an equivalent parallel capacitance of 7 pF. The Y-capacitors are chosen to be 1 nF. For the integrated CMF, the choke and the Y-capacitors are soldered directly on the power module PCB as the complete power module package; for the external CMF, the same π-type filter is connected to the power module but with a different connection setup as illustrated in Fig. 5 with different parasitic inductances.

B. Measured CM Noise Spectrum

To eliminate the differential mode noise transferring to CM noise due to the unbalance of the two power lines, a dc voltage is applied to the half bridge without any loads so that only the CM noises caused by *dv/dt* are measured in the experiment. By measuring the conduction current through the LISNs, the CM noise spectra generated by the continuous hard-switching operations under 70 V and 80 kHz of the half-bridge power module such as without filter, with an external CMF, and with the integrated CMF are obtained and compared with EMI standard CISPR 25 Class 1 peak limits as a reference in Fig. 6. The values of the parasitics from the CM equivalent circuit in Fig. 2 are measured by an impedance analyzer and listed in Table I. Fig. 6 shows that from 10 to 100 MHz, the power module with the integrated CMF shows a maximum of 50 dBμV lower EMI noise than that with the external CMF, meaning that the

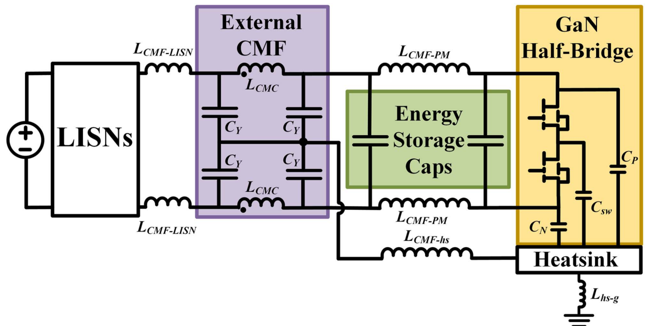

(a)

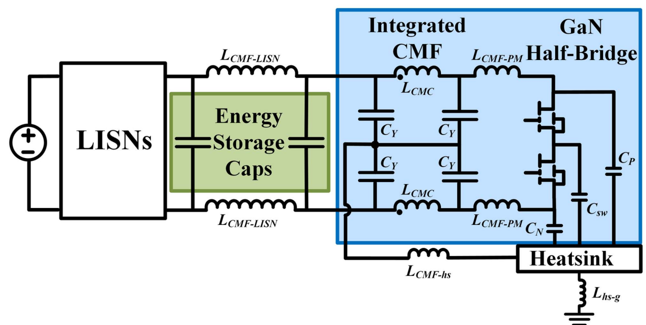

(b)

Fig. 5. Block diagrams of the experiment setups for the power module with (a) External CMF, (b) Integrated CMF.

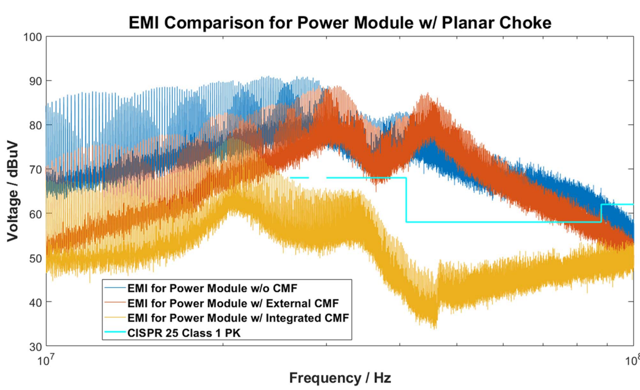

Fig. 6. CM noise spectrums comparison for the designed power module without CMF, with the external CMF, with the integrated CMF and CISPR 25 Class 1 PK.

TABLE I
MEASURED PARAMETER VALUES

Parameters	Filter Connections		
	No CMF	External CMF	Integrated CMF
$L_{CMF\text{-}PM}$ (nH)	The sum	89.37	0.42
$L_{CMF\text{-}LISN}$ (nH)	= 164.59	75.22	164.17
$L_{CMF\text{-}hs}$ (nH)	N/A	183.40	9.60
$L_{hs\text{-}g}$ (nH)	1.43	1.43	1.43
L_{CMC} (nH)	N/A	400	400
C_Y (nF)	N/A	1	1
C_{sw} (pF)	31.5	31.5	31.5
C_{PN} (pF)	38.8	38.8	38.8

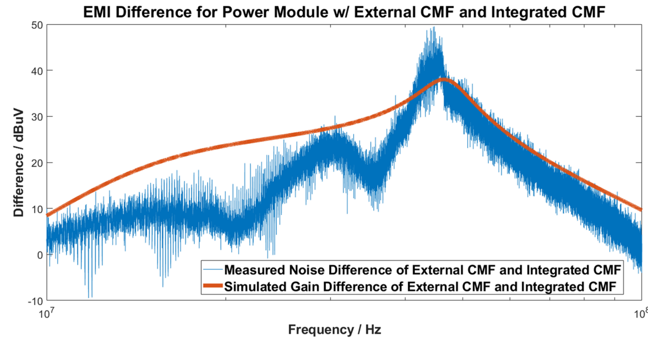

Fig. 7. Comparison of the CM noise difference between the power module with the external filter and the integrated filter from measurement and simulation. A maximum of 50 dBμV more attenuation is obtained by the integrated filter.

integrated CMF provides a higher attenuation than the external CMF in both conducted EMI frequency range and radiated EMI frequency range. The CM noise spectra generated by the power module with the integrated CMF fully satisfying the referred EMI standard further show the advantage and necessity of the integrated CMF.

C. CM Equivalent Circuit Validation

Simulation models are built in LTspice based on the CM equivalent circuits, as Fig. 2 shows under small signal ac analysis in the frequency domain, using the parameters listed in Table I. The CM voltages are measured on the LISNs' equivalent impedance for both the power module with the external CMF and then with the integrated CMF, so the LISNs' voltage insertion gains are obtained; of which the gain difference is compared with the difference of the measured EMI noises of the power module with the external CMF and integrated CMF in Fig. 7. According to Fig. 7, the simulation result matches the measured result except for some frequency points due to the resonances caused by the system parasitics and the resistive impedance mismatch, which validates the established CM equivalent circuit and its parametric study results.

IV. Conclusion

The concept of integrating EMI filters inside the power module package is discussed in this letter. Through the analysis of the CM equivalent circuit of a half-bridge power module with different parasitic inductances, it is demonstrated that the integration of CMF will achieve higher noise attenuation in the high-frequency range thanks to the shorter connections from the filter to the power module and heatsink. A GaN-based half-bridge power module package with a π-type planar CMF is designed and fabricated for validation. The measured noise spectrum shows a maximum of 50 dBμV more attenuation can be obtained with the integrated filter than with the conventional externally added filter. The simulation results are also validated by the experimental results, showing enhanced filter performance by the integration. In the future, the benefits of the CMF-integrated power module will be explored in different applications and converter topologies.

REFERENCES

[1] X. Huang, Z. Liu, F. C. Lee, and Q. Li, "Characterization and enhancement of high-voltage cascode GaN devices," *IEEE Trans. Electron. Devices*, vol. 62, no. 2, pp. 270–277, Feb. 2015.

[2] J. Sun, J. Li, D. J. Costinett, and L. M. Tolbert, "A GaN-based CRM totem-pole PFC converter with fast dynamic response and noise immunity for a multi-receiver WPT system," in *Proc. IEEE Energy Convers. Congr. Expo.*, 2020, pp. 2555–2562.

[3] J. Yao, Y. Li, S. Wang, X. Huang, and X. Lyu, "Modeling and reduction of radiated EMI in a GaN IC-based active clamp flyback adapter," *IEEE Trans. Power Electron.*, vol. 36, no. 5, pp. 5440–5449, May 2021.

[4] Z. Zhang, Y. Hu, X. Chen, G. W. Jewell, and H. Li, "A review on conductive common-mode EMI suppression methods in inverter fed motor drives," *IEEE Access*, vol. 9, pp. 18345–18360, 2021.

[5] S. Wang, F. C. Lee, D. Y. Chen, and W. G. Odendaal, "Effects of parasitic parameters on EMI filter performance," *IEEE Trans. Power Electron.*, vol. 19, no. 3, pp. 869–877, May 2004.

[6] J.-W. Shin, C.-M. Wang, and E. M. Dede, "Power semiconductor module with low-permittivity material to reduce common-mode electromagnetic interference," *IEEE Trans. Power Electron.*, vol. 33, no. 12, pp. 10027–10031, Dec. 2018.

[7] B. Cougo, H. H. Sathler, R. Riva, V. D. Santos, N. Roux, and B. Sareni, "Characterization of low-inductance SiC module with integrated capacitors for aircraft applications requiring low losses and low EMI issues," *IEEE Trans. Power Electron.*, vol. 36, no. 7, pp. 8230–8242, Jul. 2021.

[8] S. Wang, Y. Y. Maillet, F. Wang, R. Lai, F. Luo, and D. Boroyevich, "Parasitic effects of grounding paths on common-mode EMI filter's performance in power electronics systems," *IEEE Trans. Ind. Electron.*, vol. 57, no. 9, pp. 3050–3059, Sep. 2010.

[9] X. Tian et al., "An embedded GaN power module with double-sided cooling and high-density integration," in *Proc. IEEE Energy Convers. Congr. Expo* ., 2022, pp. 1–7.

[10] N. Jia, X. Tian, L. Xue, H. Bai, L. M. Tolbert, and H. Cui, "In-package common-mode filter for GaN power module with improved radiated EMI performance," in *Proc. IEEE Appl. Power Electron. Conf. Expo.*, 2022, pp. 974–979.